Orientation Dependence of Photochemical Reactions on TiO_2 Surfaces

P. A. Morris Hotsenpiller,* J. D. Bolt, and W. E. Farneth

DuPont Company, Experimental Station, Wilmington, Delaware 19880-0356

J. B. Lowekamp and G. S. Rohrer

Department of Materials Science & Engineering, Carnegie Mellon University, Pittsburgh, Pennsylvania 15213

Received: November 6, 1997; In Final Form: January 30, 1998

The photochemistry of oriented rutile surfaces has been examined using the photoreduction of Ag^+ to Ag metal from an aqueous solution onto the TiO_2 surfaces. The photochemical reaction rates and quantum yields of rutile films were found to be a function of the orientation of the rutile surface. The (100) and (110) rutile orientations have lower photoreduction rates than the (101), (111), and (001). This dependence of the photochemical reaction rates on film surface orientation is observed over a range of light intensities, illumination wavelengths, and film thicknesses. Atomic force microscopy has been used to characterize the morphologies of the film surfaces and the photoreduced Ag at these surfaces. Several properties of rutile, such as the surface morphology, surface chemistry, space charge phenomena, and charge transport, are discussed in relation to their possible contributions to the orientation dependence of the photochemistry on the rutile films.

I. Introduction

Photochemical reactions catalyzed by TiO_2 degrade pigmented paint systems[1,2] and are being investigated for use in removing contaminants from waste streams of water[3−7] and air.[8−12] In these reactions, photogenerated electrons and holes migrate to the surface of the material where they reduce acceptor and oxidize donor molecules, respectively. Most of the applications of TiO_2 photocatalysts for cleanup of waste streams utilize the oxidation half of these coupled reactions to destroy organic pollutants (for example, chlorinated hydrocarbons) in the environment. The titania photocatalysts in these systems are present in the form of particulates,[3−6,8] coatings on support materials,[9,10,12] and films on optical waveguides[7] and windows.[11]

While the reactions of the photogenerated electrons and holes in TiO_2 have been described in detail,[13−15] mechanistic understanding sufficiently complete to allow optimization of process conditions and catalyst microstructures remains an active research goal. In general terms, the photochemical reaction efficiency or quantum yield is determined by the competition between the individual reactions of the electrons and holes at the surface of the material and their recombination, both in the bulk and at the surface. The observed reduction and oxidation rates depend on the concentrations and potential energies of the photogenerated electrons and holes relative to the acceptor and donor states, respectively, at the TiO_2/medium interface as well as the rates of escape of the reaction products into the medium. Quantum yields decrease when excess charge is built up in the material due to trap sites in the lattice or when slow charge-transfer rates cause high concentrations of both electrons and holes at the surface. At steady state, the rates of all of these elementary processes are interdependent.

Several methods of decreasing and increasing the efficiencies of TiO_2 photocatalysts, while maintaining the steady-state conditions of charge neutrality (oxidation rate = reduction rate), have been investigated. Pigment manufacturers have added coatings of alumina and silica to TiO_2 particles for decades to reduce the photochemical reactivity of their pigments.[16] In applications where TiO_2 is used to oxidize organic molecules in water or air, the rate-controlling step is believed to be the charge transfer of electrons to O_2.[15] To improve the efficiency of these processes, metal atoms or clusters are added to the surface of the TiO_2 to facilitate the removal of electrons.[13,17,18] The effects of dopants in the lattice have also been examined, but the results of these studies have not always been clear. Recent work[19−23] suggests that the concentration, valence state, and phase distribution of the dopants are all important in determining their effects, making structure−activity correlations very complex. Many transition-metal dopants increase the absorption of the light and therefore the carrier concentrations but also act as recombination sites in the lattice and thereby reduce the photochemical reaction rates relative to undoped TiO_2.

The most commonly used photocatalyst material (Degussa P25) is a three-phase mixture of the amorphous, anatase, and rutile forms of TiO_2 arranged in a complex microstructure.[24] The efficiency of several photochemical processes has been optimized using P25, and anatase constitutes the greatest volume fraction of this material. Anatase is generally accepted to be more photoactive than rutile, although this may not be true for all conditions or reactions. This is believed to be due to the Fermi level of anatase being higher than that of rutile by about 0.1 eV[25] and a higher degree of surface hydroxylation in anatase. Anatase occupies a large fraction of the P25 TiO_2; however, microstructural characterization has shown that many of the particles are sheathed by a thin surface layer of rutile.[24] Therefore, many of the photochemical reactions studied using P25 material may actually be taking place at rutile surfaces.

In this paper, we report the results of our research on photochemistry at rutile surfaces with discrete orientations. Our research has primarily been conducted on surfaces produced via thin-film growth on Al_2O_3 and rutile substrates to ensure high-quality, as-grown surfaces for study and to facilitate the examination of a variety of parameters. The effects of surface

S1089-5647(98)00104-7 CCC: $15.00
Published on Web 04/02/1998

orientation, light intensity and wavelength, and film thickness will be described. This is the first report of the effect of the surface orientation of TiO_2 on its photochemical reaction rates. We will show that in the thin-film samples different surface orientations have different photoreaction efficiencies and discuss some of the structural influences that may underlie these differences. Potential mechanisms leading to these results are discussed in the context of the elementary photochemical reaction steps.

II. Experimental Procedures

A. Thin-Film Growth and Characterization. The growth and characterization techniques used to produce the thin films for this work are described briefly. For further details please see refs 26−28. The rutile films were grown using an ion-beam sputter deposition system. The vacuum chamber was evacuated to 1×10^{-7} Torr prior to deposition, and the substrates were introduced into the system through a load-lock chamber. The substrate stage was heated by halogen lamps, and the temperature was monitored by a thermocouple and an infrared pyrometer. Deposition resulted from reactively sputtering a high-purity (99.995%) Ti target with a Xe ion beam from a 3 cm Kaufmann type ion source. The ion-beam energy and current were 1000 eV and 20 mA, respectively. The growth atmosphere consisted of 1×10^{-4} Torr of Xe and 1×10^{-4} Torr of O_2. Films were grown at a substrate temperature of 725 °C and a growth rate of 3 Å/min. The thickness of most of the films used in this work was approximately 2000 Å, but films were grown with thicknesses from 15 to 2000 Å for this study.

The substrates used include (0001), $(11\bar{2}0)$, and $(10\bar{1}0)$ sapphire (Al_2O_3) and (100), (110), (101), (111), and (001) rutile. All of the substrates were epitaxially polished by the suppliers. Prior to introduction into the vacuum chamber, the substrates were rinsed with high-purity methanol. All substrates were kept in dryboxes prior to use.

The ratio of Ti to oxygen and the thickness of the films were measured using Rutherford backscattering spectrometry (RBS) of 2 MeV $^4He^+$ ions. All films on which data are reported are stoichiometric. RBS was also used to screen for any detectable impurities present in the films. The detection limits of RBS depend on the element and range from approximately 250 to 1000 ppm atomic, based on Ti, for heavier to lighter elements, respectively. The detection limits of some elements are higher due to interferences with the film and substrate compositions. Elements lighter than Al were difficult to detect in these samples. No impurities were detected in the films using RBS. X-ray diffraction was used to check the crystalline structure of the films. The surface morphology and roughness were examined by atomic force microscopy (AFM) under ambient conditions. AFM data from multiple locations on several samples have been examined to characterize the surface morphologies of each film type. The images shown are typical of what has been observed. The refractive indices of the films at 632 nm were determined using a rutile prism coupler. The indices were determined using the numerical technique developed by Ulrich and Torge.[29] The absorption characteristics were determined from unpolarized reflectance and transmission spectra measured from 350 to 830 nm on (100) rutile films.

B. Rutile Single-Crystal Annealing. Rutile single-crystal substrates of each orientation were annealed and photochemically tested for comparison to the rutile films grown on rutile and sapphire substrates. The annealing procedure consisted of the following heat treatment in air. The samples were heated to 1000 °C at a rate of 5 °C/min, then held for 2 h at 1000 °C, and cooled to room temperature at 5 °C/min. Chemical analyses of the rutile substrates were done using inductively coupled plasma spectroscopy (ICP).

C. Photochemical Reaction Rates. We have characterized the photochemical reactivity of the TiO_2 films and substrates by following the photochemical reduction of Ag^+ to Ag metal from an aqueous solution. This method of measuring reaction rates and quantum efficiencies was first described by Fleishauer, Kan, and Shepherd.[30] In our procedure, the measurements were performed in a microscope instead of a UV−visible spectrophotometer. The sample (film on substrate or substrate) was placed on a glass microscope slide with the TiO_2 film, or the surface to be tested, side up. The sample was covered in a 2.5 mm deep solution of 0.1 N $AgNO_3$ contained by an O-ring and a glass cover slip. This was placed on the microscope stage in the field of view, and the top surface of the sample was put into focus. The formation of Ag was monitored by 550 nm light from a 100 W tungsten lamp which was passed through the sample from the bottom without the use of a condenser lens, then through the 20× objective lens, and through a second 550 nm interference filter before impinging on the photodetector. UV illumination was provided by a 100 W high-pressure mercury lamp in the epi-illumination position (illumination from above) in the dark field mode (off-axis illumination). Thus, reflected light from the mercury lamp did not reach the photodetector. The light from the mercury lamp was unfiltered; both the field aperature and epi-objective aperature were wide open. A mechanical shutter blocking the mercury lamp light was initially closed to record the photodetector signal corresponding to 100% transmittance (T_0). When the shutter was opened, the transmitted light was recorded at 0.1 s intervals. Data collection was continued until the transmittance reached 98% (OD = 0.0088). These data were converted to optical density (OD = $-\log(T/T_0)$) versus time. The relative photochemical reaction rates are expressed here as the rate of change of OD, typically in units of 10^{-5}/s. The rate was determined from the slope of OD versus time for the time interval necessary to reach 99% transmittance (OD = 0.0044). For any one sample at least two different areas of the TiO_2 surface were used to determine the rate. The numbers reported for the photochemical reaction rates are the average values for all samples of a specific type.

D. Illumination Intensity and Wavelength Dependence of the Photochemical Reaction Rates. The effect of light intensity on the photochemical reaction rate was determined using the Ag^+ photoreduction technique, described above. To vary the intensity of the UV illumination, a series of neutral density filters were used. These filters were placed in the optical path of the UV source before the focusing optics. For these purposes, the intensity of UV light was determined using the transmission at 405 nm of the optical density filters, which was measured independently. This wavelength was chosen because it is the predominant wavelength (see below) of the UV illumination shorter than the absorption edge of rutile.[31,32]

The intensity of the UV light incident upon the sample as a function of wavelength was experimentally measured using a calibrated silicon photodetector combined with band-pass filters. These filters (360−370, 400−410, and 432−441 nm) isolated the principal Hg emission lines at 365, 405, and 436 nm. These measurements were done in bright field mode with a 10× objective lens to focus the UV illumination. The light intensity was corrected for the wavelength sensitivity of the detector and the illuminated area (0.126 cm^2) to calculate the incident light

TABLE 1: Orientations of Rutile Films Grown on Sapphire Substrates

film	substrate	fwhm (θ°)	fwhm (Φ°)	in-plane film || substrate	lattice mismatch, %
(100) rutile	(0001) Al_2O_3	0.20	10	[010] || [$\bar{2}$110]	3.76
				[001] || [01$\bar{1}$0]	7.27
(101) rutile	(11$\bar{2}$0) Al_2O_3	0.35	0.5	[$\bar{1}$01] \|\| [$\bar{1}$100]	0.91
				[010] || [0001]	5.78
(001) rutile	(10$\bar{1}$0) Al_2O_3	0.35	1.0	[100] || [1$\bar{2}$10]	3.6
				[010] || [0001]	5.72

intensities at each wavelength. The light intensities at 365, 405, and 436 nm are 1.1×10^{15}, 14.2×10^{15}, and 13.6×10^{15} photons/(s cm^2), respectively. The total UV ($\leq$405 nm) used in the unfiltered Ag^+ photoreduction test is roughly 15×10^{15} photons/(s cm^2). This is approximately 5 times the outdoor exposure UV intensity in direct sunlight in Florida.[33]

The number of photons absorbed by each film per second was calculated using the absorption coefficients of the applicable rutile orientations at each wavelength,[32,34] the film thickness and the incident light intensities measured as described above. Corrections were made for the reflectance off the cover glass−air and the TiO_2−water interfaces. The indices of refraction of different crystalline orientations of TiO_2 which were necessary for these corrections were calculated from data available in the literature.[35] The total reflectance from the two interfaces ranged from 18 to 24%, depending on the wavelength and the crystallographic orientation of the rutile surface.

E. Determination of the Photochemical Quantum Yields. The quantum yield was calculated as the number of Ag atoms produced by Ag^+ photoreduction divided by the total number of photons absorbed. The total number of photons absorbed was calculated by multiplying the number of photons absorbed per second at the illumination wavelength (405 or 365 nm), described above, by the time of exposure to the UV illumination. The amount of Ag formed was calculated from the size and distribution of Ag particles on the TiO_2 surfaces, measured using AFM. The areal density of Ag particles was measured in 3−5 different areas of each sample, and it was assumed that these observations were representative of the entire surface. The dimensions of 5−10 representative Ag islands in each area were measured and used to compute an average volume under the assumption that the islands were right cylinders or parallelepipeds with right angles, depending on the surface. Finally, the total amount of silver deposited was determined by assuming that each island had the density of silver metal. A detailed example of the procedure used is given in section III.B.5.

III. Results

A. Characterization of the Rutile Thin Films and Crystals. *1. Rutile Films on Sapphire Substrates.* Table 1 shows the rutile film orientations grown on the sapphire substrates[26,27] along with the X-ray diffraction full width at half-maximums (fwhm's) of the θ and Φ angles, indicating the degree of alignment of the rutile phase perpendicular to and parallel to the plane of the film. Also shown are the in-plane relationships between the film/substrate lattices and the calculated lattice mismatches between them at room temperature. The surfaces of the rutile films are oriented with the θ fwhm's between 0.20° and 0.35°. In the plane of the film, the (100) rutile has a Φ fwhm of 10° with three grain orientations present. This is due to the 3-fold symmetry in the pseudohexagonal structure of the (0001) substrate, which is not present in the (100) tetragonal rutile structure. These three grain orientations are aligned to the sapphire substrate with [010] || [$\bar{2}$110] and [001] || [01$\bar{1}$0]. The Φ scan of the (101) rutile film has a fwhm of 0.5° and indicates that there are twins present along the (101) plane in these films.[27] The (101) films are oriented relative to the sapphire substrate with [$\bar{1}$01] || [$\bar{1}$100] and [010] || [0001]. The (001) rutile film is aligned in the plane with no obvious orientational defects. The alignment of the (001) film on the substrate is [100] || [1$\bar{2}$10] and [010] || [0001].

The surface morphologies of the rutile films grown on sapphire have been characterized using AFM over a range of thicknesses.[27] Figure 1 shows the AFM images of the 2000 Å thick rutile films. Although the (100), (101), and (001) films all have an islandlike or granular morphology, they are also different from one another. The (100) film has very small features that are elongated along [010] and a surface roughness, root-mean-square (rms) value, of 4−5 Å. The surface morphology of the (101) rutile films exhibits a very distinct faceted, terrace-step structure with a typical rms roughness of 35 Å. The facets lie along [$\bar{1}$01], and the step height is approximately 9 Å. The (001) rutile film has features approximately 1000−2000 Å in size and a rms roughness ranging between 24 and 75 Å. The films (shown in Figure 1) appear to have developed morphologies that minimize their surface energies and mimic the facets on bulk crystals.[36] The (100) and (101) rutile films have significant regions of their surfaces that are quite smooth, as might be expected from their prevalence in the morphology of bulk rutile crystals (i.e., these are low surface energy planes[37]). The (001) surface is not stable, and crystals have been observed to facet on the (101) planes upon annealing at the temperature at which our films are grown.[38,39] X-ray data indicate that the edges of the features are along [100] and [010]. The AFM and SEM[26] images of the (001) film surface are consistent with a (101) type faceted morphology.

The refractive indices of the films were measured at 632 nm. The ordinary index of the films was determined to be 2.595 ± 0.089 compared to the published value of 2.584.[35] The index of the mixed ordinary and extraordinary film orientations was 2.708 ± 0.011. This is very close to the bulk value of 2.729.[35] These results indicate that the rutile films have optical indices of refraction that are comparable to those of bulk rutile crystals. The absorption edge of the (100) rutile films measured using unpolarized light at room temperature was similar to previously reported values for bulk rutile crystals (425 nm,[31] 405 nm[32]). No features were observed in the absorption spectra from the absorption edge to 830 nm.

2. Rutile Films on Rutile Substrates. Rutile films were also grown on (100), (110), (101), (111), and (001) single-crystal rutile substrates.[28] These samples were produced to provide films of the (110) and (111) rutile surface orientations, which could not be grown on sapphire, and samples of the (100), (101), and (001) orientations for comparison to those grown heteroepitaxially on sapphire substrates. The θ fwhm's of these films/substrates are typically 0.20°−0.30°. The surface morphologies of the 2000 Å thick homoepitaxial films are shown in Figure 2. Like the heteroepitaxial layers, the (100), (101), (111), and (001) films have surface morphologies that are indicative of island type growth. For example, the (100) film has islands that are approximately 1000 Å wide along [010] and 4000 Å along [001] with vertical height differences of 30−50 Å. The rms roughness is 23 Å. While the size and aspect ratio of the islands are accurately measured, their ill-defined rounded shapes are probably less realistic. Because the AFM probe tip has a finite size, closely spaced steps are imaged as continuous gradients. The islands on the (101) rutile film are comparable

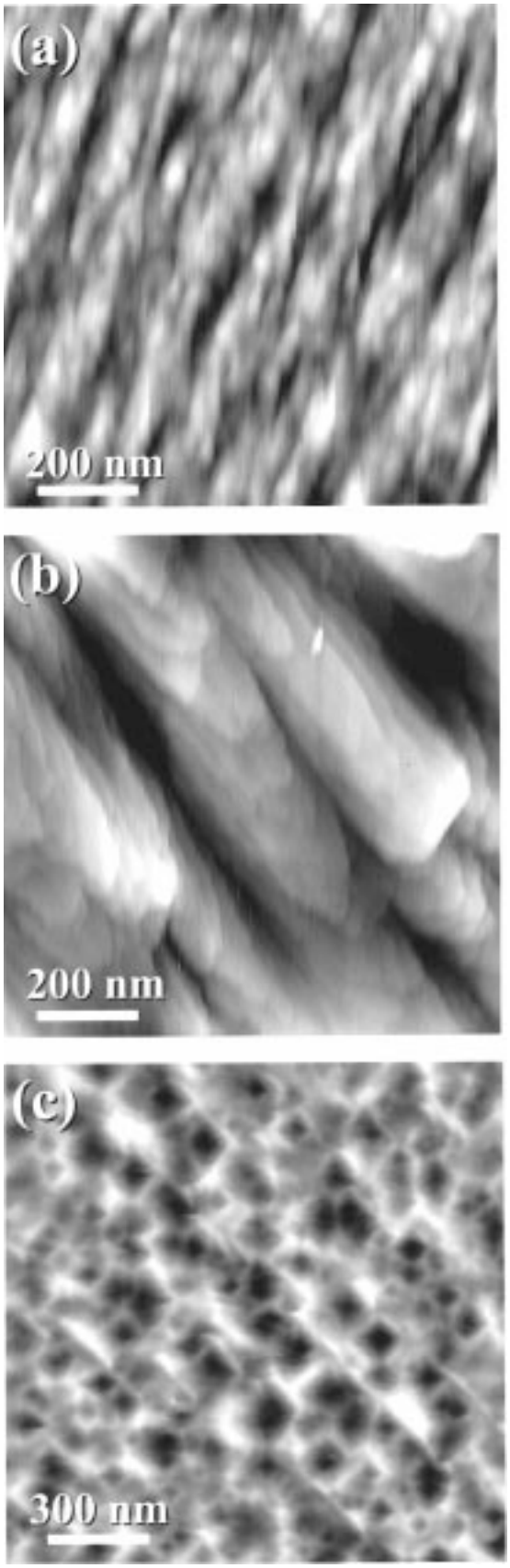

Figure 1. AFM images of 2000 Å thick rutile films grown on sapphire substrates. Images (a) (100) rutile and (b) (101) rutile represent a 1 μm × 1 μm square area. Image (c) (001) rutile is 1.5 μm × 1.5 μm. The gray scales are (a) 30 Å, (b) 90 Å, and (c) 400 Å.

in size, but they have flat equiaxed tops bounded by curved steps. The rms roughness of the (101) surface is 72−87 Å. The (111) film has an rms roughness of 135−142 Å and islands that are comparable in size to those found on the (100) and (101) homoepitaxial film surfaces. The (001) surface shows a very fine scale island structure and an rms roughness of 45−50 Å. The (110) film has a morphology that is indicative of layer-by-layer growth and is made up of a terrace-step structure with an rms roughness of 6−20 Å.

3. Rutile Single Crystals. As-polished and annealed rutile single-crystal[28] substrates with (100), (110), (101), (111), and (001) surface orientations were used to provide samples for comparison to the as-grown rutile films. The θ fwhm's of these crystals were 0.20°−0.30°. Chemical analysis by ICP indicated that the rutile crystals contained a relatively high concentration of impurities, which totaled 1.8% (mole of impurity/mole of Ti). The primary impurities were K and S. The balance was made up by small concentrations of Al, Ca, Si, and Fe.

The surfaces of the as-polished substrates were relatively smooth in some areas with rms roughnesses of 1−3 Å and few identifiable features besides some steps. However, in other areas of the as-polished substrates, polishing scratches and debris were present, and the rms roughnesses in these areas were 3−15 Å. The annealed rutile single-crystal surfaces had rms roughnesses of 1−5 Å, but the specifics of their morphologies depended on their orientation. The (100), (110), (101), and (111) annealed single-crystal surfaces had stepped morphologies consisting of several thousand angstrom wide terraces separated by small steps. On the (100) surface, the steps are 4−6 Å high, comparable to the magnitude of the lattice parameter (4.59 Å) in the [100] direction. The (110) surface has well-ordered steps on the surface that are 2 Å high. On the (101) surface, the steps are small integer multiples of the approximately 2.5 Å spacing between adjacent (101) planes. The (111) surface is very flat with steps that are 4−12 Å high. On the (100), (110), (101), and (111) surfaces, the directions of the steps varied from area to area, presumably due to small local deviations from the ideal orientation. However, the steps were always composed of straight segments meeting at corners, suggesting preference for certain low index orientations. For example, on the (10$\bar{1}$) annealed surface, the steps are aligned along [010] and [$\bar{1}$01] directions. The structure of the (001) surface was distinct from the others. It consisted of a crosshatch pattern of step features oriented along the [100] and [010] directions of the surface. Within domains, the steps exhibit a nearly periodic structure and are separated by about 100 Å.

B. Photochemistry. *1. Surface Orientation Effects on the Reaction Rates. a. Films.* Table 2 shows the photochemical reaction rates determined using the Ag^+ photoreduction technique on the (100), (110), (101), (111), and (001), 2000 Å thick, rutile films grown on sapphire and rutile substrates. In addition to the average photoreduction rates for each orientation, the standard deviation of all sample measurements of that orientation and the standard deviation per sample are listed along with the number of samples measured. It is clear from the data that the (100) and (110) rutile film orientations yield lower photoreduction rates than the (101), (111), and (001) orientations on either substrate. The difference between the least and most active samples is approximately an order of magnitude.

The film orientations grown on sapphire substrates exhibit similar relative photoactivities to those grown on rutile substrates; however, some differences are observed in the actual rates measured. The (100) rutile films grown on (0001) sapphire have a rate of 2.0×10^{-5}/s, whereas those grown on (100) rutile have a rate of 7.0×10^{-5}/s. The discrepancy may arise from

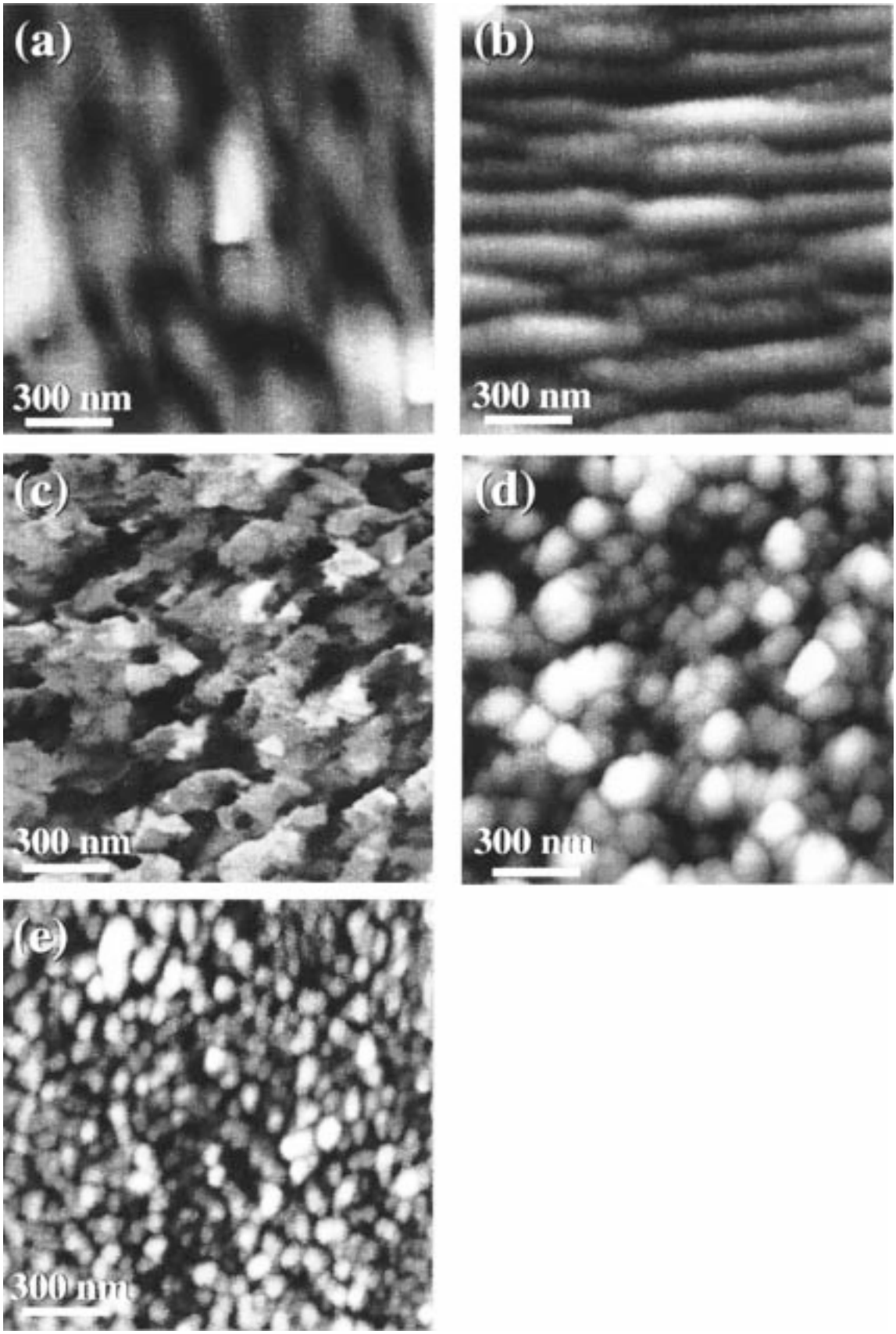

Figure 2. AFM images of 2000 Å thick rutile films grown on rutile substrates. These images are 1.5 μm × 1.5 μm square. Image (a) (100) rutile has a 80 Å gray scale, (b) (110) rutile a 25 Å verticle scale, (c) (101) rutile a 175 Å gray scale, (d) (111) rutile a 500 Å scale, and (e) (001) rutile a 150 Å gray scale.

the larger variability in the results of the (100) films grown on the rutile substrates and the fact that only two of these samples have been measured. The limited number of samples is due to the difficulty in obtaining defect-free rutile crystal substrates of this orientation. The average rates measured on the (101) and (001) rutile films grown on sapphire and rutile are more

TABLE 2: Ag^+ Photoreduction Rates (10^5/s) of 2000 Å Thick Rutile Films: Surface Orientation Effects

film	substrate	av rate all samples	std dev rate all samples	std dev rate per sample	no. of samples
(100) rutile	(0001) sapphire	2.0	±0.6	±0.4	10
	(100) rutile	7.0	±2.0	±3.0	2
(110) rutile	(11$\bar{0}$) rutile	3.0	±1.6	±0.8	5
(101) rutile	(11$\bar{2}$0) sapphire	20	±12	±4	11
	(101) rutile	13	±4	±4	3
(111) rutile	(11$\bar{1}$) rutile	13	±4	±4	5
(001) rutile	(10$\bar{1}$0) sapphire	30	±12	±6	9
	(001) rutile	17	±6	±8	4

comparable; however, in these cases the films grown on rutile substrates are approximately 40% less active.

Ag^+ reduction rates measured on the (100), (101), and (001) rutile films grown on sapphire substrates in the absence of the UV illumination source were approximately 2 orders of magnitude lower than those reported in Table 2, indicating that the reaction rates measured during irradiation are primarily determined by the photoinitiated reduction of Ag^+ ions. Ag^+ photoreduction can also be observed on uncoated sapphire substrates. The maximum rates on the (0001), (11$\bar{2}$0), and (10$\bar{1}$0) sapphire substrates were 1.2×10^{-5}, 0.5×10^{-5}, and 1.6×10^{-5}/s, respectively. The photoreduction rates of (100) rutile films grown on sapphire may have some contribution from the (0001) substrates, but clearly the orientational differences measured are not reflections of the substrate differences. Very little of the photoreduction is attributable to the sapphire.

b. Rutile Crystal Substrates. The photoreduction rates measured on as-polished rutile crystal substrates (with no film on the surface) were all similar and rather high ($(20-30) \times 10^{-5}$/s). No orientation effect was observed for the photoreduction rates of these samples. The annealed rutile crystal substrates had photoreduction rates that were all relatively low ($(1.4-5.3) \times 10^{-5}$/s), and again no orientation effect was observed. Oriented rutile substrates were obtained from two different suppliers for this study, and similar photochemical results were obtained with both materials. These results are in contrast to those obtained on the rutile thin films.

Some of the factors that may contribute to the orientation-dependent photochemical reactivity of the rutile films will be discussed in section IV. We would now like to address the question of how the polished and annealed rutile substrate surfaces differ from those of the films and why these differences lead to orientation-independent photochemical reactivity. The polished surfaces of rutile single-crystal substrates are flat relative to the films with an rms roughness of 1−15 Å compared to 5−150 Å for rutile films of various orientations. However, this does not mean that the polished surfaces are defect-free on the atomic scale. Polishing leaves high concentrations of extended defects (i.e., dislocations) and point defects (vacancies and interstitials) that are randomly distributed over the surface as well as scratches that are 10−20 Å deep. After irradiation of the polished crystals, the Ag particles are observed to form preferentially in these damaged areas.

Annealing the substrates removes the polishing defects and creates terrace-step morphologies on the surfaces. The photoactivity drops by about an order of magnitude upon annealing. Chemical analyses of the rutile substrates revealed that they contained high levels of impurities, which totaled 1.8% (mole of impurity/mole of Ti). The impurity concentrations are likely to be enhanced at the surfaces of the annealed substrates since it is known that typical impurities in rutile segregate on heating. AFM images show particulate impurities at the surfaces after annealing, prior to irradiation, and it is likely that nonparticulate concentrations of impurites not resolved by AFM are more widely present over the surface. These changes in surface composition could be responsible for the reduced photochemical reaction rates.[19−23] Impurity concentrations in the films are at least an order of magnitude lower than this. We believe that the impurities at the surfaces of the annealed substrates mask the orientation effects observed with both heteroepitaixal and homoepitaxial films. Annealed rutile crystals containing impurity concentrations comparable to the films should exhibit orientation-dependent photoreduction rates like those of the epitaxial films.

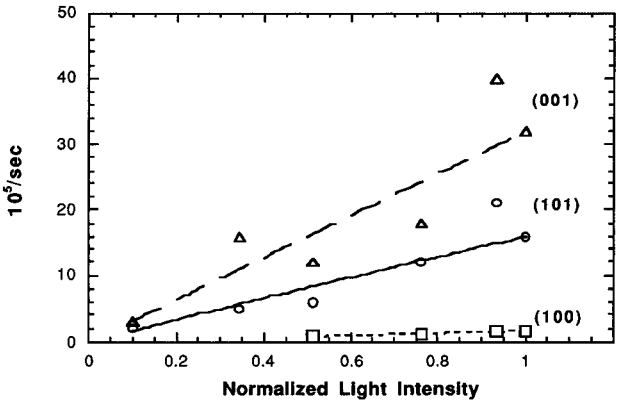

Figure 3. Photochemical reaction rates of the, 2000 Å thick, (100), (101), and (001) rutile films grown on sapphire substrates plotted as a function of normalized light intensity ($\lambda = 405$ nm).

The film surfaces are also rougher than the polished rutile substrate surfaces, and the additional roughness is due to surface topographical features that are similar to those found on the annealed rutile substrates. The film surfaces are characterized by microfacets that have formed to lower the surface energy relative to the energy of the growth plane. The greater rms roughness is a measure of the extension of these facets above and below the average growth plane. Although the edges and corners between these microfacets are types of defects, a greater rms roughness does not necessarily imply higher concentrations of these types of coordination sites relative to the polished crystals. As on the annealed substrate surfaces, the surface morphologies of the films are relaxed by the conditions of growth and have a relatively low energy. Therefore, the rutile films provide surfaces that have few impurities present and morphological features that are similar to those found on the surfaces of the annealed rutile substrates.

2. Effect of the Illumination Intensity. The average photochemical reaction rates measured on the (100), (101), and (001), 2000 Å thick, rutile films grown on sapphire substrates as a function of the normalized light intensity ($\lambda = 405$ nm) are shown in Figure 3. The intensity of the illumination with no neutral density filter present was set to 1.0. The reaction rates are clearly a linear function of the intensity in all three film orientations. The data for each orientation were fit with the equation $y = kx^b$. For the (100), (101), and (001) films the exponents, b, were 0.91, 0.97, and 1.0, respectively. The correlation coefficients were 0.99, 0.93, and 0.90. The values of k were 1.6×10^{-5}, 16×10^{-5}, and 32×10^{-5}/s. These results indicate that the reaction rates are not controlled by recombination processes in any of these orientations. If recombination played a dominant role, then the exponent would be expected to be ≤ 0.5.[15] The effect of surface orientation on the photochemical reaction rates is evident in these data over the light intensity range examined. The constant k in the

TABLE 3: Photoreduction Rates (10^5/s) of 2000 Å Thick Rutile Films: Wavelength Effects

film	substrate	365 nm as-measured	365 nm corrected	405 nm as-measured
(100) rutile	(0001) Al_2O_3	0.16	0.74	1.4
(101) rutile	(11$\bar{2}$0) Al_2O_3	0.45	2.1	4.2
(001) rutile	(10$\bar{1}$0) Al_2O_3	1.6	7.4	9.9

equation is affected by both the absorption of the films and their quantum yields. The k ratios of the (101) and (001) orientations to that of the (100) orientation are 10 and 20, respectively. The ratios, (101)/(100) and (001)/(100), of the absorption coefficients at 405 nm[32] of rutile corrected for reflective losses are 1.0 and 1.3, respectively. Therefore, the differences in the values of k appear to have more to do with differences in the quantum yields of the different film surface orientations than their absorption coefficients.

3. Effect of the Illumination Wavelength. Table 3 shows the results of measurements of the photoreduction rates of 2000 Å thick films grown on sapphire using only 365 nm (column 3) or 405 nm light (column 5). To compare the wavelength effect independent of differences in the number of photons absorbed at the two wavelengths, the photoreduction rates measured at 365 nm were multiplied by the ratio of the intensities of the light absorbed at 405 nm to that at 365 nm. This correction assumes that the rates are linearly dependent on the illumination intensity at both wavelengths, as suggested in Figure 3. The corrected values of the photoreduction rates measured at 365 nm are given in column 4 in Table 3. The corrected photoreduction rates at 365 nm and those measured at 405 nm are within a factor of 2 of each other. This is good agreement, given the assumptions, and we conclude that the photochemistry is not significantly dependent on the energy of the absorbed photon in this wavelength range. The surface orientation effect on the Ag^+ photoreduction rates is present at both wavelengths, as well.

4. Effect of Film Thickness. The effect of rutile film thickness on the photoreduction rates is shown in Figure 4. The (101) and (001) films used for these data were grown on sapphire substrates. The photoreduction rates here were determined using all the light available from the mercury lamp. The data appear to exhibit two regimes of behavior with the break occurring at approximately 100 Å thick for each orientation. If the dependence on thickness is assumed to be linear at thicknesses $\geq$100 Å, the slopes of the lines are 0.00069×10^{-5} and 0.0012×10^{-5}/(s Å) for the (101) and (001) films, respectively. The ratio, (001)/(101), of the slopes is 1.74. At thicknesses $\leq$100 Å, there appears to be a much steeper increase in the photoreduction rates with thickness. The slopes of the lines drawn through the (101) and (001) data are 0.12×10^{-5} and 0.18×10^{-5}/(s Å), respectively, and the ratio, (001)/(101), of the slopes of these lines is 1.54. The correlation coefficients of the lines drawn through the data are all $\geq$0.95. The ratios of the slopes in both thickness regimes are comparable.

At constant illumination, the plot of rate of reaction vs film thickness has a slope that is proportional to the quantum yield times the absorptivity. The ratio, (001)/(101), of the absorption coefficients[32] of these rutile orientations corrected for reflective losses is 1.3. The ratio of the observed reaction rates is in the same direction and somewhat larger than this in both thickness regimes. The observed break in the data at thicknesses in the range of 100 Å could result from an increased absorption coefficient in the near surface region of the material. For example, surface states could have different absorption characteristics. However, for the change in behavior to be due to absorption only, the surface state absorptivity ratio and the bulk

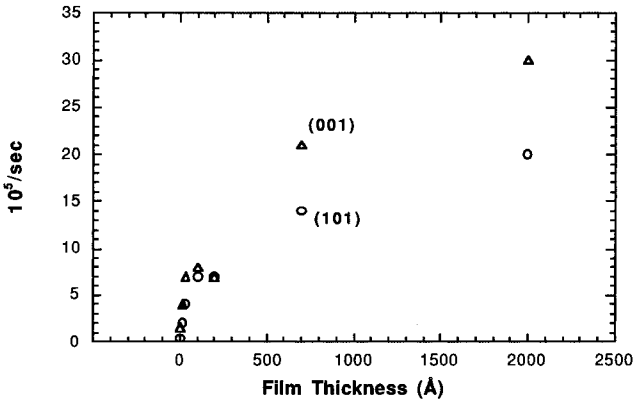

Figure 4. Photochemical reaction rates of the (001) and (101) rutile films grown on sapphire substrates plotted as a function of rutile film thickness.

absorptivity ratio would have to be the same since the ratio of the slopes of the rate vs thickness plots is the same in the two regimes. To rationalize Figure 4, it seems likely that the quantum yields must be both thickness- and orientation-dependent.

The slopes of the data in Figure 4 may get shallower at thicknesses greater than approximately 100 Å because the quantum yield is decreasing as the films get thicker and the photons are absorbed further from the surface. This could result in an increase in the recombination rate during electron and hole transport to the surface. Space charge effects could increase the quantum yield in the $\leq$100 Å thickness range.[40,41] Space charge potentials can produce higher quantum yields when the absorption process is occurring in a thickness regime comparable to the space charge potential because of more efficient charge separation. Another effect that could contribute to higher quantum yields in very thin films ($\leq$100 Å) results from the nanometer size and morphology of these films. Previous work[27] has shown that the rutile films on sapphire grow heteroepitaxially with an island type mechanism producing morphologies with features resembling half-particles (100−500 Å diameter) on the substrate surface at thicknesses below 100 Å. Discrete particles of TiO_2 (<100 Å) on quartz substrates were shown to have enhanced photoactivities.[42] Nanometer size particles of TiO_2 have been observed to exhibit quantum size effects that result from a larger band gap of small particles. This produces an enhancement of the activities of electrons and holes or an increased rate constant for charge transfer.[42,43]

Tada and Tanaka[7] observed a linear increase in the photochemical reaction rates of sol−gel-derived TiO_2 films on quartz with increasing thickness up to approximately 1400 Å, using film-surface illumination. Above this thickness, the photochemical rates plateaued or decreased. Their results suggested that the crystallinity and defects present in the sol−gel films had a large influence on the photochemistry. These sol−gel films were also not oriented and would not be expected to exhibit the same behavior as the epitaxial films used here.

5. Quantum Yields. Quantum yields for Ag^+ photoreduction determined from combined light intensity and AFM measurements on the (100), (101), and (001), 2000 Å thick, rutile films grown on sapphire substrates are shown in Table 4. AFM has been used to estimate the number of Ag atoms produced under a given set of irradiation conditions. The data clearly indicate that the (100) rutile surface has a much lower quantum yield than the (101) or (001) surfaces. Recently, the techniques used to determine quantum yields in heterogeneous photocatalytic systems were reviewed and in many cases found to ignore

TABLE 4: Quantum Yields of 2000 Å Thick Rutile Films

		quantum yields[a]		
film	substrate	405 nm (0.0088)	405 nm (0.0022)	365 nm (0.0044)
(100) rutile	(0001) Al_2O_3	0.06		0.03
(101) rutile	(11$\bar{2}$0) Al_2O_3	0.5	0.6	0.4
(001) rutile	(10$\bar{1}$0) Al_2O_3	≥ 1[b]	≥ 1[b]	0.9

[a] The 405 or 365 nm wavelengths shown were the UV illumination used. The optical density (OD, in parentheses) given above each column was determined using the 550 nm monitoring illumination. [b] The quantum yields are reported as ≥ 1 because it was very difficult to differentiate the Ag islands from the film surface topograpy. The values of the quantum yields in these cases are essentially 1.

effects such as the illumination wavelength, light scattering, and concentration which can significantly affect the calculated yields.[44] Below is a detailed description of the methods and calculations we have used to determine the quantum yields shown in Table 4 which we believe address these concerns.

Parts a and b of Figure 5 show two (101) rutile film surfaces that have been exposed to 405 nm light for times sufficient for the transmittance at 550 nm to reach 99.5% (OD = 0.0022) and 98% (OD = 0.0088), respectively. The incident photon flux at this wavelength, corrected for wavelength sensitivity of the detector, was 1.79×10^{15} photons/s. After corrections for reflective losses off the cover glass−air and TiO_2 water−interfaces, the photon flux (1.43×10^{15} photons/s) was multiplied by the absorption coefficient, thickness of the film, and exposure time and divided by the illumination area to determine the number of photons absorbed. The number of photons absorbed by the films shown in Figure 5a,b was 11.8×10^{14} and 72.6×10^{14} photons/cm^2, respectively. Analysis of the AFM images in Figure 5 indicates that the Ag particle densities are 3×10^8 and 5×10^8/cm^2, respectively. In general, there is a good correlation between the amount of deposited Ag determined by AFM and the photoreduction rates determined by transmittance changes. A more detailed comparison would require information about the size and shape dependence of the absorbance of the Ag particles at 550 nm. Assuming that the Ag particles, or white areas in the images (Figure 5a,b), are right cylinders, the average volume of the particles increases from 5×10^{-17} to 21×10^{-17} cm^3. The calculated surface concentrations of Ag on the (101) surfaces shown in Figure 5a,b are 1×10^{-9} and 7×10^{-9} mol/cm^2, respectively. The calculated quantum efficiencies, or the ratio of Ag atoms produced to photons absorbed, for the two samples are in the range 0.5−0.6.

The accuracy of the quantum yields shown in Table 4 is dependent on the validity of the assumptions discussed in Section II.E and the ability to distinguish the correct size of the Ag islands from the film morphologies using AFM. Because of the finite size of the AFM probe, the lateral dimensions of features protuding from the surface are systematically overestimated. However, for the flat, disk-shaped islands observed here (the lateral dimensions of the Ag particles are typically 20 times larger than their height), this error is not considered significant. Because of the small number of Ag particles on the (100) films and the morphology of the (001) films, we expect that the density of islands was determined with less certainty than on the (101) films. However, the quantum yields determined at different levels of transmittance, or conversion of Ag^+ to Ag, on the (101) and (001) orientations using 405 nm light were similar, suggesting that the techniques used to calculate the number of Ag atoms formed and the number of photons absorbed are, at least, consistent. The quantum yields measured for each rutile surface using 365 nm light were comparable to those determined using 405 nm light, which is consistent with the lack of a wavelength effect on the reaction rates (Table 3).

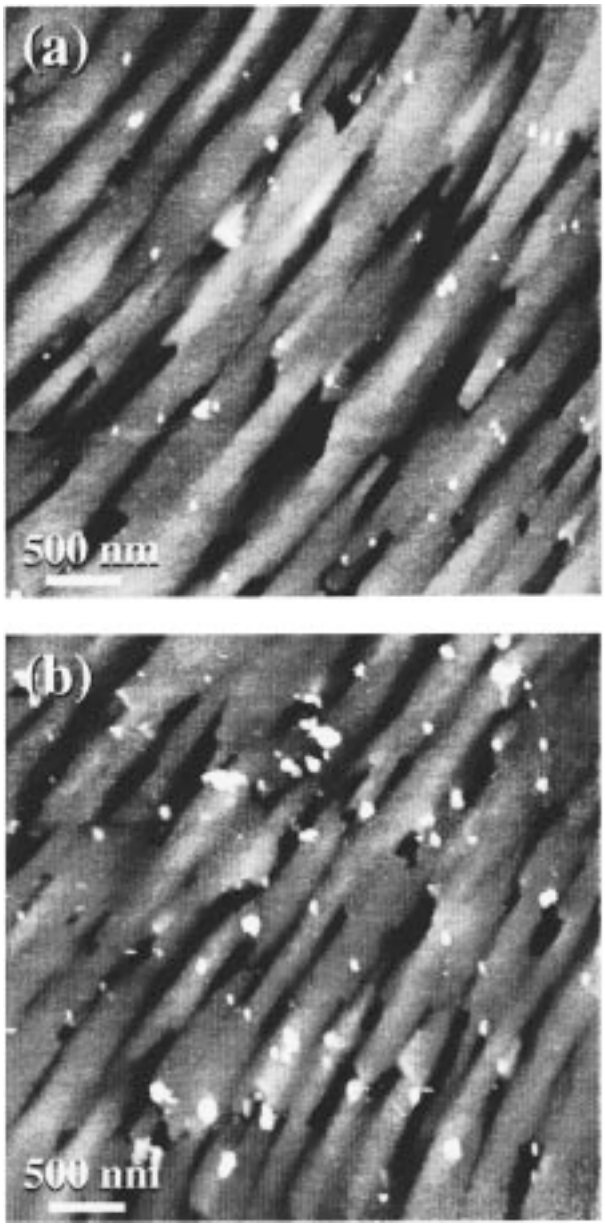

Figure 5. AFM images of 2000 Å thick rutile films after the Ag^+ photoreduction test. The films were exposed to 405 nm light for times sufficient for the transmittance to reach (a) 99.5% (OD = 0.0022) and (b) 98% (OD = 0.0088). The white regions in each image are Ag particles deposited on the surface. The calculated surface concentrations of Ag on the surfaces are (a) 1×10^{-9} mol/cm^2 and (b) 7×10^{-9} mol/cm^2. The calculated quantum efficiencies of the two samples were in the range 0.5−0.6. Both images are 4 μm × 4 μm and have gray scales of 100 Å.

IV. Discussion: Factors Contributing to the Effect of Surface Orientation on the Photochemistry

Data presented in previous sections clearly demonstrate that TiO_2 rutile films of differing orientations show differing photochemical activity in our Ag^+ photoreduction protocol. The (100) and (110) rutile film orientations have lower photoreduction rates than the (101), (111), and (001). The difference observed between the least (100) and most active (001), 2000 Å, thick film orientations is approximately an order of magni-

tude. Furthermore, our observations imply that these differences in photoreduction rate are not the result of differences in the rate of electron−hole pair generation, but rather the efficiency with which electron−hole pairs created in different film orientations can be used to initiate photochemistry. The difference in the quantum yields (Table 4) of these rutile film surfaces is also approximately an order of magnitude. The dependence of the photochemical reaction rates and quantum yields on the surface orientation of the rutile films may result from a variety of material properties, including the surface morphology, surface chemistry, space charge phenomena, and charge transport. Many of these properties are interrelated and can contribute to the photochemical reaction rates in several ways. Below, we examine some of the potential effects of each.

A. Surface Morphology. The surface morphology could contribute to the orientation dependence of the photochemical reaction rates or quantum yields through differences in the surface area, Ti site density, and Ti coordination on the specific facets present. Simple models of the surface morphologies of the (100), (101), and (001), 2000 Å thick, rutile films grown on sapphire (Figure 1) were used to calculate the surface area per unit area of the AFM topographs. For example, the (001) oriented film was approximated by 0.1 × 0.1 μm inverted pyramids with depths equal to 0.04 μm covering the surface. The calculated surface areas of the (100), (101), and (001) films were 1.0, 1.5, and 2.6 $\mu m^2/\mu m^2$, respectively. The differences in surface area do not appear to explain the order of magnitude difference between the reaction rates or quantum yields of the least (100) and most (001) photochemically reactive surfaces. The Ti site densities of the surfaces were calculated by multiplying the site densities[45] of the facets present on the surfaces by their specific surface areas. The calculated Ti site densities of the (100), (101), and (001) orientations were 7.4, 11.5, and 20.2/nm^2, respectively. It should be pointed out, however, that the Ti sites on each surface are not necessarily expected to be equivalent. Each of the films is expected to have predominantly 5-coordinate Ti on the exposed facets, but the calculated surface energy of the (101) surface is greater than that of the (100) surface.[37] Although the surface area, Ti site density, and surface energy are not independent of one another, all three quantities are larger for orientations with higher photochemical reaction rates.

The only measured surface morphological factor of the rutile films on sapphire substrates that varies by the same magnitude as the photochemical reaction rates and yields is the rms roughness. The (100), (101), and (001) surfaces of the, 2000 Å thick, rutile films grown on sapphire substrates have rms roughnesses which are 4−5, 35, and 24−75 Å, respectively. The rms roughness is defined as the root-mean-square of the deviation in height of the surface as determined by AFM. In this case, the rms roughness is a measure of the relative size of the out-of-plane features on the film surfaces, such as facets with orientations different from the growth orientation. The differences between the films are obvious when one considers the vertical scales of the images in Figure 1. Vertical height differences on the (001) oriented film are about 10 times greater than on the (100) film, and this means that a relatively larger fraction of the exposed surface is composed of facets with out-of-plane orientations. These out-of-plane orientations and the surface features that accompany this rougher morphology may result in a larger variety of surface coordination environments, some of which may be particularly photochemically reactive.[14,42,46] However, the rms roughnesses of the (100), (110), (101), (111), and (001), 2000 Å thick, rutile films grown on rutile substrates are 23, 6−20, 72−87, 135−152, and 45−50 Å, respectively. Because the rms roughnesses of these films do not correlate to their measured photoreduction rates, the rms roughness itself is clearly not an adequate measure of the relative photochemical reactivity of rutile surfaces.

B. Surface Chemistry. The differences observed in the photochemical reactivities and quantum yields of the rutile film surfaces could also be due to differences in their surface chemistries, such as the mechanisms of adsorption and desorption or the specific reactions taking place. In studies of rutile single crystals with the (001) orientation, the product distributions in the reactions of primary alcohols and carboxylic acids are found to be determined primarily by the coordination environment of individual Ti ions.[47−51] The (001) surface can facet into {101} or {114} type structures.[38,39] Five-coordinated Ti ions are exposed on both surfaces, whereas four-coordinated Ti ions are only found on the {114} facets. Dimethyl ether was produced from methanol via disproportionation of pairs of methoxides coordinated to 4-fold-coordinated Ti ions on the {114} faceted surface, whereas no detectable quantities of dimethyl ether were produced at the {101} type surface.[48] The {101} faceted (001) surface also did not produce ethers from ethanol, 1-propanol, or 2-propanol.[49] In studies of the reactions of acetic acid on the (001) surface, the bimolecular reaction of surface acetates to form acetone was observed to occur only on the {114} structure.[50] Analogous reactions took place on the {114} faceted surface with propionic acid and acrylic acid.[50,51] These results clearly indicate that thermally activated chemistry occurring at the surfaces of rutile is a strong function of the specific sites present, particularly the concentration of Ti ions with reduced oxygen coordination (Ti^{3+} defects). The coordination of Ti at the surfaces of rutile has also been observed to affect the adsorption characteristics of water, H_2, and CO.[52−54] Water is found to be associatively adsorbed on fully oxygenated (100) and (110) surfaces of rutile but tends to dissociate into surface hydroxyl groups on Ti^{3+}-rich surfaces.[52,53] These defects also act as adsorption sites for H_2 and CO.[54]

The presence of defects on the surfaces of rutile may also affect their photochemical reactivities. Specific sites could facilitate the binding and/or charge transfer of photoinduced electrons and holes to acceptors (Ag^+) and donors (OH^-), respectively. The orientation effect on the photochemical reaction rates and yields could be due to differences in the concentrations of specific local coordination environments (defect sites) at each of the rutile film surfaces.

C. Space Charge and Charge Transport Phenomena. Space charge effects could play a significant role in determining the photochemical reaction rates and quantum yields of rutile film surfaces. Space charge potentials can produce higher quantum yields when the absorption process generates electron−hole pairs within the space charge layer, due to more efficient charge separation and reduced recombination.[40,41] Assuming that the space charge potential exponentially decays from the surface, the Debye length is the characteristic distance describing the depth of the affected region.[55,56] The Debye length is dependent on a variety of factors, including the dielectric constant of the material. Therefore, the difference in the dielectric constants of rutile ($\epsilon(0) = 170$ parallel to [001] and 86 parallel to [100][32]) could contribute to the differences observed in the photochemical reaction rates at rutile film surfaces. From this analysis, the space charge region at the (001) surface would be expected to be approximately 1.5 times the size of the region at the (100) surface, all other factors assumed constant. When the space charge region is smaller

than the absorption depth, the carriers are created in a region not affected by the space charge potential, and the probability of recombination increases, thereby decreasing the quantum efficiency of the process.[40] The precise magnitude of this effect is difficult to determine, but it may contribute to the order of magnitude difference in the photochemical quantum yields at the rutile film surfaces.

Assuming Frenkel defects in rutile and a free energy of formation for vacant Ti sites which is greater than that for titanium interstitials, the sign of the space charge potential in nonirradiated rutile would be positive and the surface potential would be negative.[55,56] This implies that the concentration of electrons is relatively high at the surfaces. The magnitude of the surface potential would affect both the space charge depth and the adsorption of molecules at the surface.[41]

Charge transport to the surfaces of rutile is most likely dominated by traps at room temperature. The Hall mobility of photogenerated electrons along [001] in rutile was found to be approximately 1.5 times greater than the mobility of the holes and is approximately 2.5 times greater than along [100].[32] Higher mobilities along [001] in rutile could contribute to higher photochemical reaction rates and yields at surfaces containing a component of this direction normal to their plane.

The rutile lattice is made up of edge- and corner-sharing TiO_6 octahedra that lie in rows and form channels parallel to [001]. No channels are present perpendicular to [001]. The diffusion coefficient of Li^+ ions parallel to [001] in rutile is at least 10^8 times greater than the coefficient perpendicular to [001].[57] Anisotropy is also found in the diffusion of H^+ ions.[58] The activation energy for diffusion of H^+ along [001] is one-half that for diffusion perpendicular to [001].[58] If migration of H^+ ions were necessary for charge compensation in the rutile lattice as part of the photochemical process, this anisotropy in ion diffusion coefficients may also affect the photochemical rates and quantum yields.

V. Conclusions

Our results clearly show that photocatalytic reaction rates are different on differently oriented crystalline rutile films. Furthermore, the differences are probably related to differences in the efficiency of electron−hole pair utilization rather than electron−hole pair creation. We have not attempted to develop a specific explanation or model for the orientational dependence of the photochemistry. Rather, we have briefly reviewed several of the properties of rutile that could influence the rates of the photochemical reactions under steady-state conditions. It is interesting that most of the properties of the rutile films suggest an orientation effect with the (001) surface having a greater photochemical reactivity than (100). Consideration of the surface areas, Ti site densities, surface chemistries, dielectric constants, space charge potentials, carrier mobilities, and ion diffusivities all imply higher reactivity for (001) surfaces.

Acknowledgment. The authors would like to thank G. A. Wilson and D. J. Jones for experimental assistance during the course of this work. Portions of this material are based upon work supported under a National Science Foundation Graduate Fellowship. Additional support at CMU was provided by a National Science Foundation GOALI supplement (DMR-9712606) to YIA Grant DMR-9458005. RBS measurements were done using the facility at the Laboratory for Research on the Structure of Matter at the University of Pennsylvania.

References and Notes

(1) Pappas, S. P.; Fischer, R. M. *J. Paint Technol.* **1974**, *46*, 65.
(2) Volz, H. G.; Kaempf, G.; Fitzky, H. G.; Klaeren, A. *Photodegradation and Photostabilization of Coatings*; The American Chemical Society: Washington, DC, 1981; p 163.
(3) Ohtani, B.; Okugawa, Y.; Nishimoto, S.; Kagiya, T. *J. Phys. Chem.* **1987**, *91*, 3550.
(4) Augugliaro, V.; Loddo, V.; Palmisano, L.; Schiavello, M. *J. Catal.* **1995**, *153*, 32.
(5) Martin, S. T.; Lee, A. T.; Hoffmann *Environ. Sci. Technol.* **1995**, *29*, 2567.
(6) Zhang, Y.; Crittenden, J. C.; Hand, D. W.; Perram, D. L. U.S. Patent No. 5,501,801, 1996.
(7) Tada, H.; Honda, H. *J. Electrochem. Soc.* **1995**, *142*, 3438.
(8) Dibble, L. A.; Raupp, G. B. *Catal. Lett.* **1990**, *4*, 345.
(9) Dibble, L. A.; Raupp, G. B. *Environ. Sci. Technol.* **1992**, *26*, 492.
(10) Nimios, M. R.; Jacoby, W. A.; Blake, D. M.; Milne, T. A. *Environ. Sci. Technol.* **1993**, *27*, 732.
(11) Fujishima, A.; Hashimoto, K.; Kubota, Y. J. *Surf. Sci. Soc. Jpn.* **1995**, *16*, 188.
(12) Sattler, M. L. Rates of Photocatalytic Oxidation of Organic Compounds in Air over Titanium Dioxide. Ph.D. Thesis, University of Texas, Austin, TX, 1996.
(13) Gerischer, H.; Heller, A. *J. Phys. Chem.* **1991**, *95*, 5261.
(14) Gerischer, H.; Heller, A. *J. Electrochem. Soc.* **1992**, *139*, 113.
(15) Gerischer, H. *Photocatalytic Purification and Treatment of Water and Air*; Ollis, D. F., Al-Ekabi, H., Eds.; Elsevier: New York, 1993; p 1.
(16) Werner, A. J. U.S. Patent No. 3,437,502, 1968.
(17) Magrini, K. A.; Watt, A.; Rinehart, B. *Sol. Eng.* **1995**, *1*, 415.
(18) Takaoka, Y.; Hirobe, Y.; Tomonari, M.; Kinoshita, Y. Eur. Pat. Appl. 95101593.2, 1995.
(19) Navio, J. A.; Colon, G.; Litter, M. I.; Bianco, G. N. *J. Mol. Catal.* **1996**, *A106*, 267.
(20) Elfenthal, L.; Schwindt, R.; Kluwig, M. U.S. Patent No. 5,451, 252, 1995.
(21) Serpone, N.; Lawless, D.; Disdier, J.; Herrmann, J.-M. *Langmuir* **1994**, *10*, 643.
(22) Choi, W.; Termin, A.; Hoffmann, M. R. *J. Phys. Chem.* **1994**, *98*, 13669.
(23) Martin, S. T.; Morrison, C. L.; Hoffmann, M. R. *J. Phys. Chem.* **1994**, *98*, 13695.
(24) Bickley, R. I.; Gonzalez-Carreno, T.; Lees, J. S.; Palmisano, L.; Tilley, R. J. D. *J. Solid State Chem.* **1991**, *92*, 178.
(25) Maruska, H. P.; Ghosh, A. K. *Sol. Energy* **1978**, *20*, 443.
(26) Morris Hotsenpiller, P. A.; Wilson, G. A.; Roshko, A.; Rothman, J. B.; Rohrer, G. S. *J. Cryst. Growth* **1996**, *166*, 779.
(27) Morris Hotsenpiller, P. A.; Roshko, A.; Lowekamp, J. B.; Rohrer, G. S. *J. Cryst. Growth* **1997**, *174*, 424.
(28) Giocondi, J.; Lowekamp, J. B.; Rohrer, G. S.; Morris Hotsenpiller, P. A. In *Integrated Thin Films and Applications*; Pandey, R. K., Morris Hotsenpiller, P. A., Roshko, A., Varshney, U., Witter, D. E.; Eds.; Ceramic Trans: Westerville, OH, 1998; Vol. 8b, in press.
(29) Ulrich, R.; Torge, R. *Appl. Opt.* **1973**, *12*, 2901.
(30) Fleischauer, P. D.; Alan Kan, H. K.; Shepherd, J. R. *J. Am. Chem. Soc.* **1972**, *94*, 283.
(31) Tang, H.; Berger, H.; Schmid, P. E.; Levy, F. *Solid State Commun.* **1994**, *92*, 267.
(32) Goodenough, J. B.; Hamnett, A.; Huber, G. Hulliger, F.; Leib, M.; Ramasesha, S. K.; Werheit, H. In *Landolt-Bornstein, Numerical Data and Functional Relationships in Science and Technology*; Hellwege, K.-H., Madelung, O., Eds.; Springer-Verlag: New York, 1984; Vol. 17, Subvol. g., Chapter 9.15.2.1, p 133.
(33) Egerton, T. A.; King, C. J. *J. Oil Col. Chem. Assoc.* **1979**, *62*, 386.
(34) The ratio of the absorption coefficients of rutile films at 365 nm to those at 405 nm was determined from the measurements of the absorption edges of the (100) rutile films. The measured absorption coefficients at 405 nm were set to the published values.[32]
(35) Dodge, M. J. In *Handbook of Laser Science and Technology, Optical Materials: Part 2*; Weber, M. J., Ed.; CRC Press: Boca Raton, FL, 1986; Vol. IV, p 15.
(36) Dana, J. D.; Dana, E. S. *The System of Minerology*; John Wiley: New York, 1944; p 554.
(37) Ramamoorthy, M.; Vanderbilt, D.; King-Smith, R. D. *Phys. Rev. B* **1994**, *49*, 16721.
(38) Firment, L. E. *Surf. Sci.* **1982**, *116*, 205.
(39) Kurtz, R. L. *Surf. Sci.* **1986**, *177*, 526.
(40) Salvador, P. *J. Appl. Phys.* **1984**, *55*, 2977.
(41) Bickley, R. I. *Chem. Phys. Solids Their Surf.* **1978**, *7*, 118.
(42) Anpo, M.; Shima, T.; Kodama, S.; Kubokawa, Y. *J. Phys. Chem.* **1987**, *91*, 4305.
(43) Hoffmann, M. R.; Martin, S. T.; Choi, W.; Bahnemann, D. W. *Chem. Rev.* **1995**, *95*, 69.
(44) Serpone, N. J. *Photochem. Photobiol. A: Chem.* **1997**, *104*, 1.
(45) Jones, P.; Hockey, J. A. *Trans. Faraday Soc.* **1971**, *67*, 2679.

(46) Pichat, P. *Photochemical Conversion and Storage of Solar Energy*; Pelizzetti, E., Schiavello, M., Eds.; Kluwer: Dordrecht, The Netherlands, 1990; p 277.
(47) Lusvardi, V. S.; Barteau, M. A.; Farneth, W. E. *J. Catal.* **1995**, *153*, 41.
(48) Kim, K. S.; Barteau, M. A. *Surf. Sci.* **1989**, *223*, 13.
(49) Kim, K. S.; Barteau, M. A. *J. Mol. Catal.* **1990**, *63*, 103.
(50) Kim, K. S.; Barteau, M. A. *J. Catal.* **1990**, *125*, 353.
(51) Idriss, H.; Kim, K. S.; Barteau, M. A. *Structure−Activity and Selectivity Relationships in Heterogeneous Catalysis*; Grasselli, R. K., Sleight, A. W., Eds.; Elsevier: Amsterdam, 1991; p 327.
(52) Lo, W. J.; Chung, Y. W.; Somorjai, G. A. *Surf. Sci.* **1978**, *71*, 199.
(53) Hugenschmidt, M. B.; Gamble, L.; Campbell, C. T. *Surf. Sci.* **1994**, *302*, 329.
(54) Gopel, W.; Rocker, G.; Feierabend, R. *Phys. Rev. B* **1983**, *28*, 3427.
(55) Ikeda, J. A.; Chiang, Y. M. *J. Am. Ceram. Soc.* **1993**, *76*, 2437.
(56) Ikeda, J. A.; Chiang, Y. M.; Garratt-Reed, A. J.; Vander Sande, J. B. *J. Am. Ceram. Soc.* **1993**, *76*, 2447.
(57) Johnson, O. W. *Phys. Rev.* **1964**, *136*, 284.
(58) Johnson, O. W.; Paek, S.-H.; DeFord, J. W. *J. Appl. Phys.* **1975**, *46*, 1026.